

Effect of Chloride on Localized Corrosion Initiation of Carbon Steel in a CO₂ Aqueous Environment

Xin Gao, Bruce Brown, Srdjan Nesic

Institute for Corrosion and Multiphase Technology

Ohio University, Athens, OH 45701

ABSTRACT

This research was focused on the effect of chloride on the initiation of localized corrosion on carbon steel in a CO₂ aqueous environment. The investigation was approached using a two-stage experimental design. The first stage was to build a protective FeCO₃ layer on the steel surface in an electrolyte with a low concentration of the salt (NaCl or NaClO₄) by purging CO₂ and adding additional ferric ions for a high initial FeCO₃ saturation condition. The second stage was to challenge the FeCO₃ layer by adding additional salt (NaCl or NaClO₄), where the effects of different salts could be compared. For both stages, linear polarization resistance (LPR) measurement was performed to measure the general corrosion rate during the experiment followed by weight loss measurement for general corrosion rate and optical profilometry measurements for localized corrosion rate after the experiment. In addition, X-ray diffraction (XRD) and scanning electron microscope (SEM) were used to analyze the composition and morphology of the corrosion product layer.

The results showed that localized corrosion was initiated in the experiments that were conducted at 80°C and 0.53 bar pCO₂ with a 1.7 molar (10 wt. %) NaCl. However, almost identical results were obtained when using NaClO₄ with the same ionic strength as NaCl. This indicated that changing the ionic strength of the solution, which led to the change of the solubility of iron carbonate, was the key to initiate localized corrosion, rather than the specific type of anion used.

Keywords: pitting corrosion, CO₂ corrosion, sodium chloride, sodium perchlorate, ionic strength, iron carbonate

INTRODUCTION

Mild steel is widely used as pipeline materials in oil and gas industry. The susceptibility of mild steel to internal localized corrosion in the pipelines with CO₂ aqueous environments significantly challenges the integrity of the pipelines. Localized corrosion can be divided into two major stages: initiation and propagation.¹

One mode of propagation of localized CO₂ corrosion has been previously studied and described by some researchers.^{2,3,4} Han used an artificial pit apparatus which allowed direct in situ measurement of the galvanic current. In that research, the potential on the iron carbonate covered surface was found to be more positive than the potential of the bare steel surface and, when connected in situ, 'localized corrosion' would continue under certain environmental conditions. This study provided proof that localized corrosion could propagate and grow in a CO₂ corrosion environment when an initiation process occurred that would partially damage the iron carbonate layer to leave a small bare steel area coupled with the larger iron carbonate covered surface area.

However, the initiation processes for localized CO₂ corrosion have not been diligently studied. There are a variety of mechanical and chemical factors that could be linked to localized corrosion. Factors related to the water chemistry include chloride concentration ([Cl⁻]), presence of organic acids, and low pH. In the oil and gas industry, high [Cl⁻] is often found in the produced water.^{5,6} Cheng's research⁷ showed that [Cl⁻] helped promote the breakdown of the carbon steel's passive film which was formed in NaHCO₃ solution. Sun's investigation⁸ indicated that initiation of localized corrosion was related to [Cl⁻] because it affected the solubility of the protective layer by changing the ionic strength of the bulk solution. Fang's research⁵ revealed that both the anodic and cathodic reaction processes were affected by [Cl⁻] and the general corrosion rate decreased with the increase of [Cl⁻]. Some researchers suggested that [Cl⁻] was directly related to localized pitting corrosion,⁹ but others⁸ expressed an opinion that [Cl⁻] role was to significantly change the ionic strength of the solution, which affects the solubility of a protective iron carbonate (FeCO₃) layer and indirectly leads to localized corrosion. Therefore, it is still unknown exactly how or if chlorides play a role in the initiation of localized corrosion in CO₂ environments.

To investigate the mechanism of initiation of localized corrosion by chlorides in a CO₂ aqueous environment, the following hypothesis was examined first:

“Initiation of localized CO₂ corrosion can be caused by a change in the chloride concentration of the solution.”

The pathway was thought to be related to a partial breakdown of a protective iron carbonate layer on mild steel surface which would occur either due to change in the solubility of iron carbonate due to increase in the ionic strength or may be directly related to the addition of chlorides. Both possibilities were reviewed.

EXPERIMENTAL PROCEDURE

A 2 L glass cell with a three electrode system for polarization resistance measurements and four isolated hanging samples for weight loss measurements were used for each experiment, as shown in Figure 1. The working electrode and weight loss samples were made from X65 pipeline steel. The electrochemical system used a platinum counter electrode and a Ag/AgCl reference electrode. For each experiment, six X65 mild steel samples were simultaneously exposed to the CO₂ purged aqueous salt solution at the beginning of the experiment and were removed at different times for analysis.

A repeatable set of environmental conditions were created in each experiment to cause a protective iron carbonate layer to form on the metal surface and rapidly reduce the corrosion rate. FeCO₃ will precipitate when the concentrations of ferrous and carbonate ions in solution exceed the solubility limit of FeCO₃ as shown by the reaction in Equation (1). The saturation value of iron carbonate ($S_{(FeCO_3)}$) is the criterion often used¹⁰ to determine if FeCO₃ should precipitate (for $S_{(FeCO_3)} > 1$) or dissolve (for $S_{(FeCO_3)} < 1$), and is calculated according to Equation (2). The $K_{sp(FeCO_3)}$ is the solubility product constant for FeCO₃, which is a function of temperature and ionic strength (I) of the solution.¹¹



$$S_{(FeCO_3)} = \frac{C_{Fe^{2+}} C_{CO_3^{2-}}}{K_{sp(FeCO_3)}} \quad (2)$$

$$K_{sp(FeCO_3)} = 10^{-59.3498 - 0.041377 \times T - \frac{2.1963}{T} + 24.5724 \times \log(T) + 2.518 \times I^{0.5} - 0.067 \times I} \quad (3)$$

Each experiment had two stages:

- 1) an FeCO₃ layer building stage used to develop a repeatable starting point, and

- 2) an FeCO_3 layer breakdown stage when an abrupt change in the salt concentration was made which was expected to lead to the breakdown of the FeCO_3 layer.

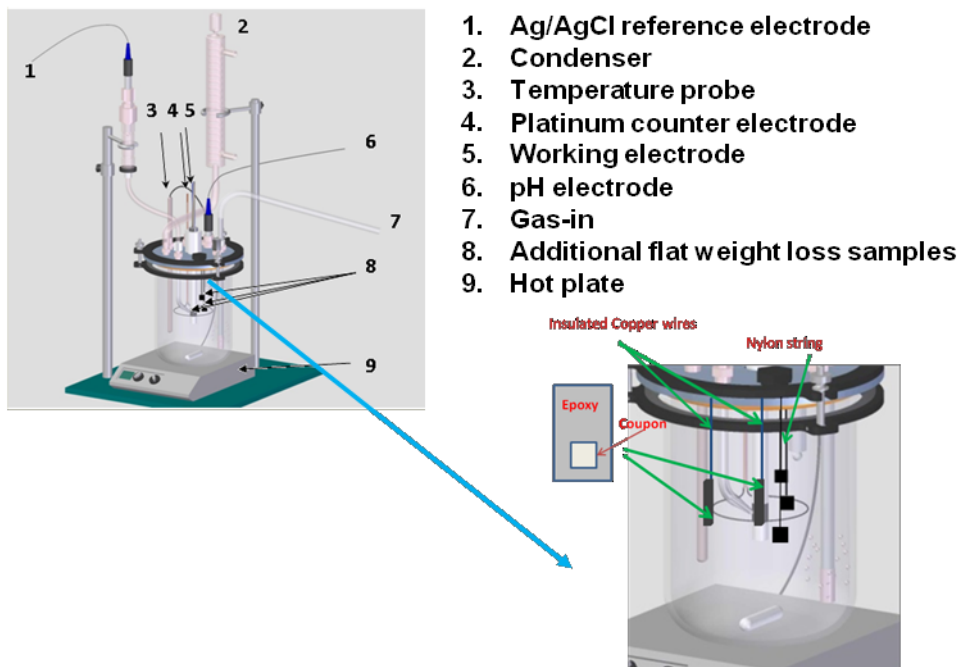


Figure 1: Glass cell set-up

During the first stage, a designated amount of Fe^{2+} (as $\text{FeCl}_2 \cdot 4\text{H}_2\text{O}$) was injected into the glass cell to accelerate the precipitation of FeCO_3 by increasing the saturation value of FeCO_3 to a high value. The precipitation of FeCO_3 covered the mild steel surface causing the general corrosion rate to decrease rapidly to around 0.1mm/yr. Pseudo-passivation of the mild steel surface occurred which was indicated by an increase in the open circuit potential (OCP). At this point, the first stage was completed as the iron carbonate layer fully covered the sample surface. Then a crystalline salt was added into the system to begin the second stage of the experiment.

In this work, two types of salt (sodium chloride NaCl and sodium perchlorate NaClO_4) solutions were used as the electrolyte. While choice of NaCl was obvious, the reason why NaClO_4 was chosen in addition will be explained in Part II of the Results section below.

The test matrix for experiments using a NaCl solution is shown in Table 1 and the test matrix for the experiments using a NaClO_4 solution is shown in Table 2. For each experiment, the solution was purged with CO_2 , the temperature was set at 80°C (176°F), and then the solution pH was adjusted using a deoxygenated 1 M NaHCO_3 aqueous solution. The samples were polished with 150, 400 and 600 grit sand paper sequentially, rinsed with isopropanol and then dried by a cool air blower before insertion into the glass cell.

For each experiment, linear polarization resistance (LPR) measurements were made (using a Gamry* Reference 600 potentiostat) to determine a general corrosion rate, once every few hours. A Thermo Scientific GENESYS* 10 Vis Spectrophotometer was used to measure dissolved Fe^{2+} concentration once every day. Scanning electron microscopy (SEM) and an optical profilometry were used to analyze the corrosion product film, and X-ray diffraction (XRD) was used to determine the corrosion product chemical composition.

* Tradename

Table 1
Test matrix for experiments using a NaCl solution

Solution	NaCl (wt. %)	Experiment 1		Experiment 2		Experiment 3		Experiment 4	
	Days	0.1	→ 1	0.1	→ 3	1	→ 10	1	→ 15
Temperature (°C)		2.5	13.5	2	21	3	6	1.5	12.5
pH (initial)		80		80		80		80	
CO ₂ partial pressure (bar)		6.6		6.6		6.6		6.6	
Total Pressure (bar)		0.53		0.53		0.53		0.53	
Saturation of [FeCO ₃] _{initial}		1		1		1		1	
Experiment time (days)		680		680		600		600	
Material		16		23		9		14	
Electrochemical measurements		X65		X65		X65		X65	
Surface morphology		LPR							
		SEM, Optical Profilometry, XRD							

Table 2
Test matrix for experiments using a NaClO₄ solution

Solution	1 wt% NaClO ₄ (initially), after the protective FeCO ₃ formed for 2 days then more salt was added for a 21 wt% NaClO ₄ (same ionic strength of 1.75 as 10 wt. % NaCl).
Temperature (°C)	80
pH (initial)	6.6
Total Pressure (bar)	1
Saturation value of [FeCO ₃] _{initial}	745 (100 ppm Fe ²⁺)
Total time (days)	14
Material	X65
Electrochemical measurements	LPR
Surface morphology	SEM, Optical Profilometry, XRD

RESULTS and DISCUSSION

Part I: Experiments in a NaCl solution

Corrosion behavior

The variance of general corrosion rates for four different experiments is shown in Figure 2. In each of the four, after additional Fe²⁺ ions were added, the corrosion rate decreased rapidly and became stable at around 0.1 mm/yr, which meant that a protective iron carbonate layer formed. The corrosion potential also increased indicating pseudo-passivation of the steel surface. When more solid NaCl was added into the glass cell, the corrosion rate increased immediately and the corrosion potential decreased significantly, which indicated that the iron carbonate layer experienced breakdown and lost some protective characteristics.

Initial protective FeCO₃ layer formation (stage 1)

Figure 3 shows the topography of the FeCO₃ layer developed in Experiment 2 under following conditions: 0.1 wt.% NaCl solution, 80°C (176°F), initial pH 6.6, pCO₂ 0.53 bar, which was composed of prismatic FeCO₃ along with plate-like crystals. Figure 4 shows the cross-section of the surface layer of Experiment 2. The layer seems to be dense, thick and protective with some general corrosion that occurred beneath the precipitated layer. It should be noted that the surface morphology and the cross-section of the layer formed in Experiment 1 were very similar to the one formed in Experiment 2.

Figure 5 shows the FeCO₃ layer topography developed in Experiment 3 under following conditions: 1 wt.% NaCl solution, 80°C (176°F), initial pH 6.6, pCO₂ 0.53 bar, which was composed of a dense layer of FeCO₃ prisms. The cross section in Figure 6 shows that the layer was dense and adhered to the metal with a thickness of around 7µm without much general corrosion seen underneath. The surface morphology and the cross-section of the layer formed in Experiment 4 were very similar to the one formed in Experiment 3.

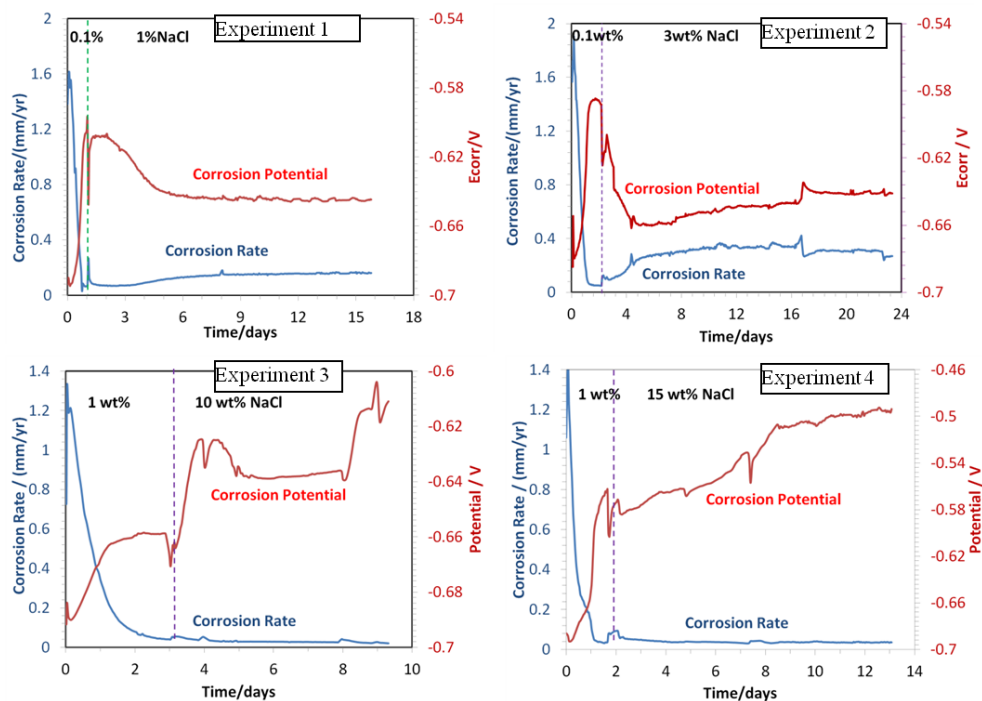


Figure 2: Variation of corrosion rate and corrosion potential with time as determined by LPR measurements

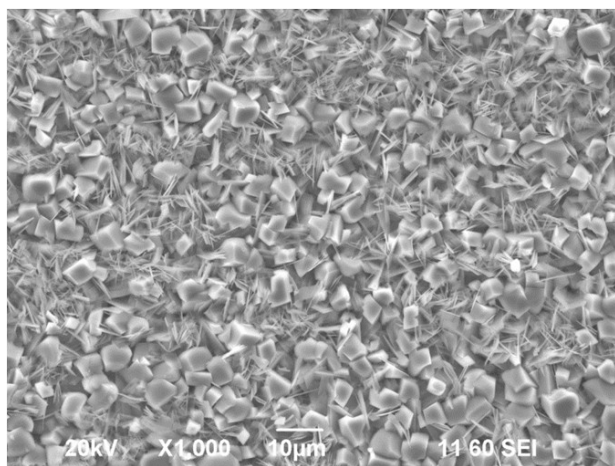


Figure 3: Surface morphology after FeCO_3 building process of Experiment 2 (0.1 wt. % NaCl solution, 80°C (176°F), initial pH 6.6, $p\text{CO}_2$ 0.53 bar)

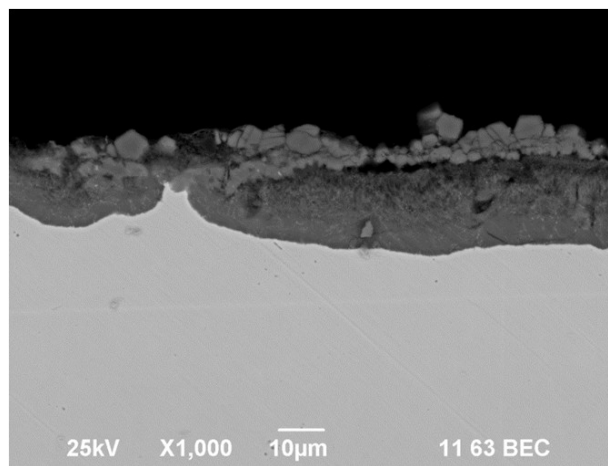


Figure 4: Cross-Section analysis after FeCO_3 building process of Experiment 2 (0.1 wt. % NaCl solution, 80°C (176°F), initial pH 6.6, $p\text{CO}_2$ 0.53 bar)

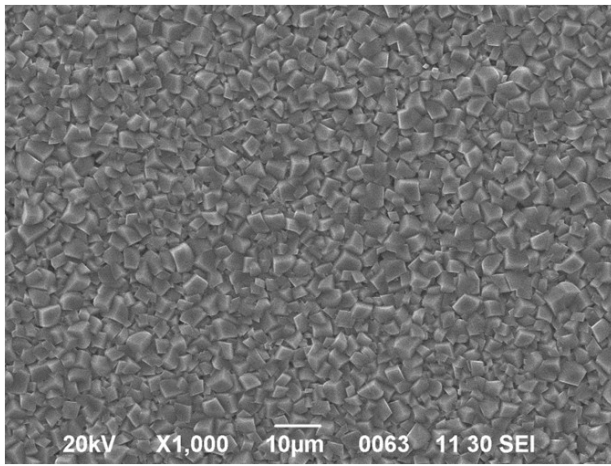


Figure 5: Surface morphology after FeCO₃ building process of Experiment 3 (1 wt. % NaCl solution, 80°C (176°F), initial pH 6.6, pCO₂ 0.53 bar)

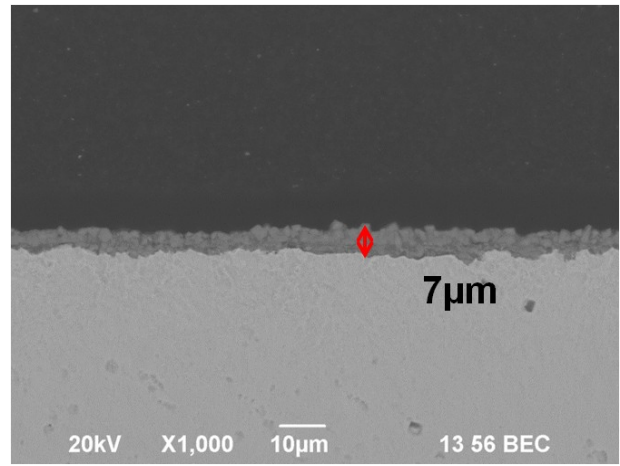
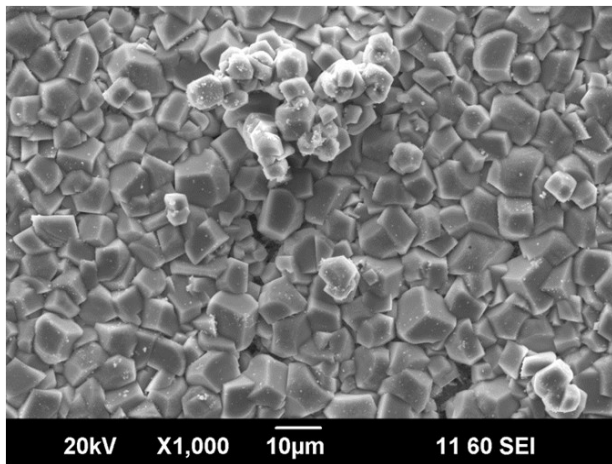


Figure 6: Cross-Section analysis after FeCO₃ building process of Experiment 3 (1 wt. % NaCl solution, 80°C (176°F), initial pH 6.6, pCO₂ 0.53 bar)

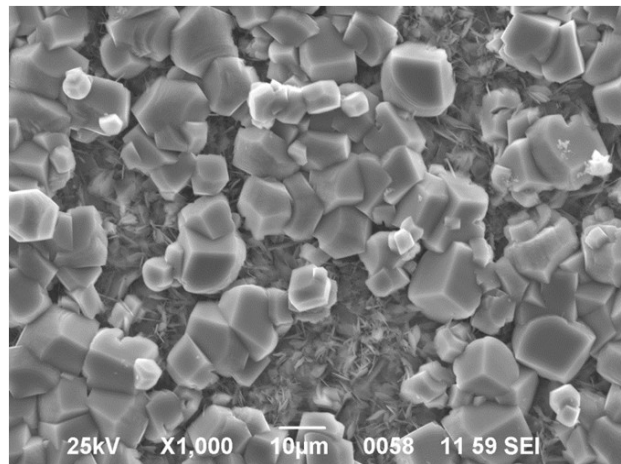
These images of the FeCO₃ layer developed in stage 1 of each experiment indicate that there was a good repeatability to form the initial corrosion product layer that would be challenged by the increased chloride concentration in stage 2.

Breakdown of protective FeCO₃ layer (stage 2)

The surface morphologies at the end of the Experiments 1 & 2 are shown in Figure 7. Figure 7a is for Experiment 1 after the formed FeCO₃ layer was exposed to a 1wt.% NaCl aqueous solution for 13.5 days. It indicates that the FeCO₃ plates were the first to dissolve back into solution. Figure 7b is for Experiment 2 after the FeCO₃ layer was exposed to the 3wt.% NaCl solution for 21 days and also shows only FeCO₃ prisms remained. The cross-section morphology of the FeCO₃ layer formed in Experiment 1, as shown in Figure 8a, displays that the layer was still dense with a thickness of 21 µm and that there was no observable pitting corrosion. Figure 8b is the cross-section morphology of the FeCO₃ layer formed in Experiment 2, which is the same sample as in Figure 7b. In this case, it looks like the FeCO₃ layer was generally attacked with part of iron carbonate crystals missing and corrosion of the metal substrate, but no pitting corrosion was found.

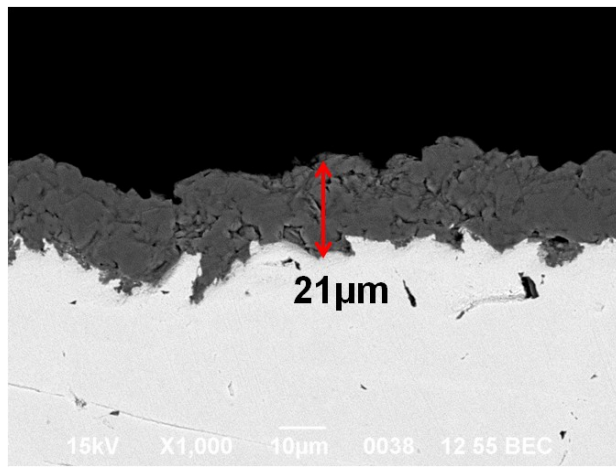


(a)

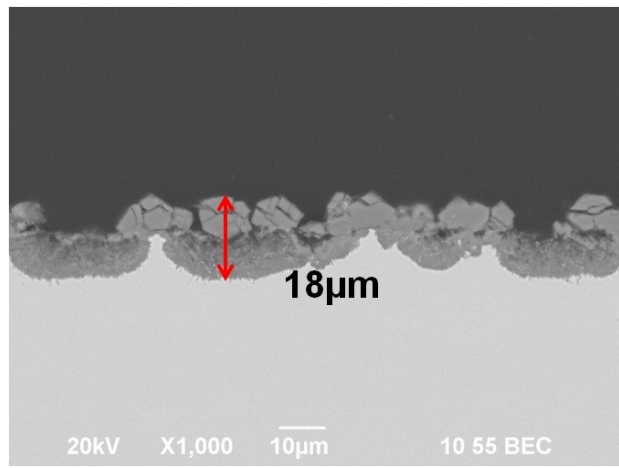


(b)

Figure 7: Surface morphology after breakdown of FeCO₃ for (a) Experiment 1 (b) Experiment 2



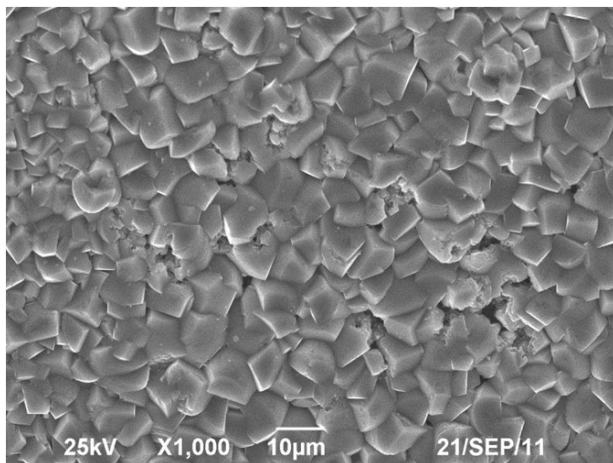
(a)



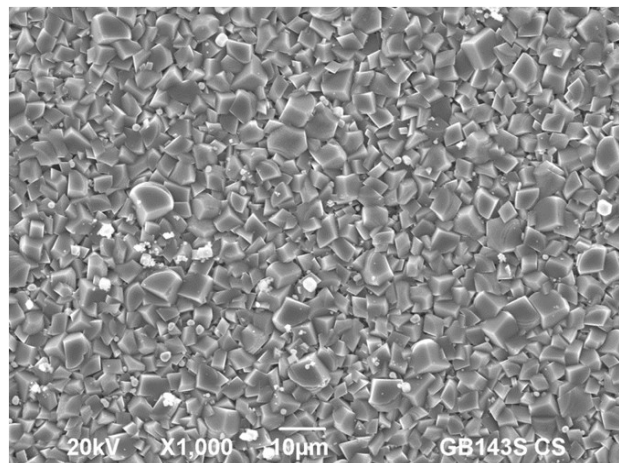
(b)

Figure 8: Cross-section after breakdown of FeCO₃ for (a) Experiment 1 (b) Experiment 2

The surface morphologies at the end of Experiments 3 & 4 are shown in Figure 9. Figure 9a is for Experiment 3 after the FeCO₃ layer formed in stage 1 was exposed to the 10 wt.% NaCl solution for 6 days; it indicates that FeCO₃ was locally dissolved. Figure 9b is for Experiment 4 after FeCO₃ was exposed to the 15wt. % NaCl solution for 12.5 days. Interestingly, the morphology is still similar to that in Figure 5 before adding additional salt. Figure 10a shows the cross-section morphology of the FeCO₃ layer at the end of Experiment 3, for the same sample seen in Figure 9a. It seems that the FeCO₃ layer was greatly affected by the change in NaCl concentration, as indicated by the presence of localized corrosion up to a depth of 13 μm penetration. Figure 10b is the cross-section morphology of the FeCO₃ layer at the end of Experiment 4, for the same sample seen in Figure 9b. It also indicates the failure of the FeCO₃ layer to act as a protective barrier to corrosion and reveal pits with penetration depths up to 17 μm.



(a)



(b)

Figure 9: Surface morphology after adding additional NaCl for (a) Experiment 3 (b) Experiment 4

Optical profilometry analysis

The surface morphology of the steel surface after removal of corrosion product layer using Clarke solution¹² for Experiments 1 & 2 are shown in Figure 11. Several locations were analyzed and the maximum depth of pits found for both Experiments was 7μm. Based on this depth value, the pitting penetration rate was calculated to be 0.14 mm/yr for Experiment 1 and 0.1 mm/yr for Experiment 2. The general corrosion rates obtained from weight loss was 0.13 mm/yr for Experiment 1 and 0.3 mm/yr for Experiment 2. Thus, the ratio of the pitting penetration rate vs. the general corrosion rate (called: pitting ratio) calculated for Experiment 1 was 1.2 and for Experiment 4 was 0.3, which means that no localized corrosion was found in these two Experiments.

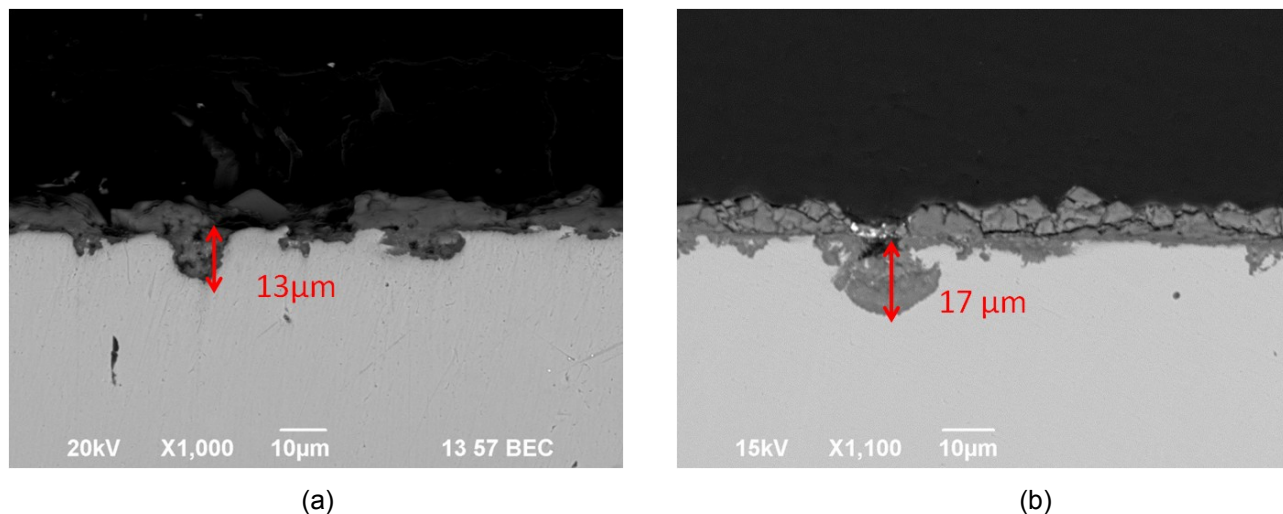


Figure 10: Cross-section after breakdown of FeCO_3 for (a) Experiment 3 (b) Experiment 4

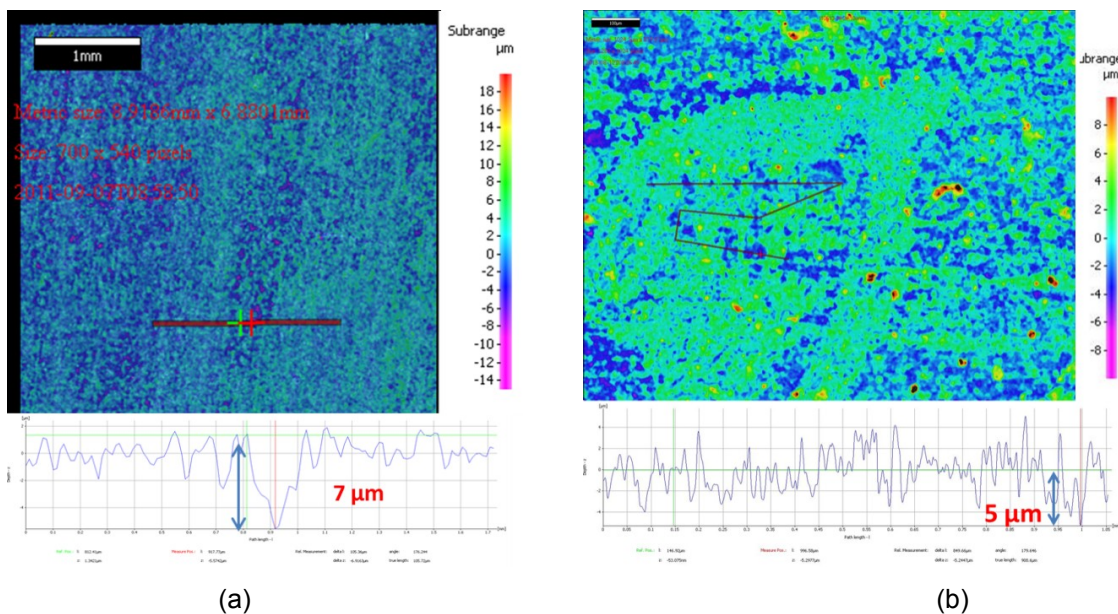


Figure 11: Optical profilometry images and analysis of the steel surface after removal of corrosion product layer (a) Experiment 1 (b) Experiment 2

The surface morphology of the steel surface after removal of corrosion product using Clarke solution for Experiments 3 & 4 are shown in Figure 12. After scanning several locations, the deepest pit observed for Experiment 3 was $14 \mu\text{m}$ and for Experiment 4 was $13 \mu\text{m}$. Based on this depth value and the general corrosion rates obtained from weight loss, the pitting ratio for Experiment 3 was 19 and for Experiment 4 was 7.3. Because the pitting penetration rate was more than 5 times larger than the general corrosion rate, it is considered that localized corrosion was found in Experiments 3 and 4. Therefore, the optical profilometry results agreed with the results obtained from SEM cross-section analysis.

Corrosion rate comparison

A comparison of general corrosion rates obtained from LPR measurements and weight loss measurements for Experiments 1 through 4 is shown in Figure 13. It indicates that with an increase in concentration of NaCl in solution, the general corrosion rate decreased. This result was in agreement with Fang's experimental results⁵.

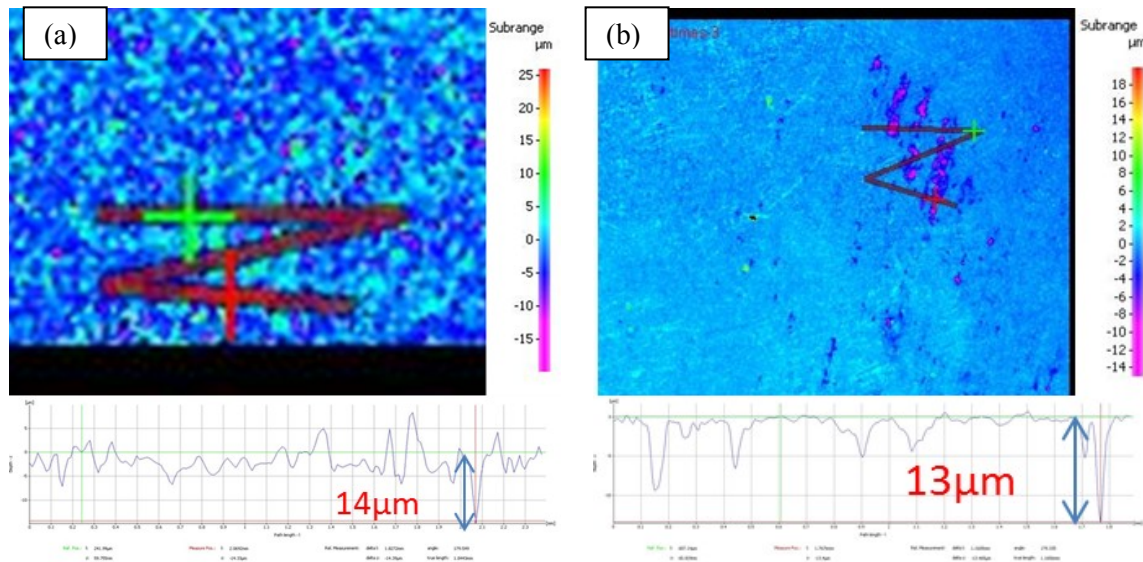


Figure 12: Optical Profilometry images and analysis of the steel surface after removal of corrosion product layer
 (a) Experiment 3 (b) Experiment 4

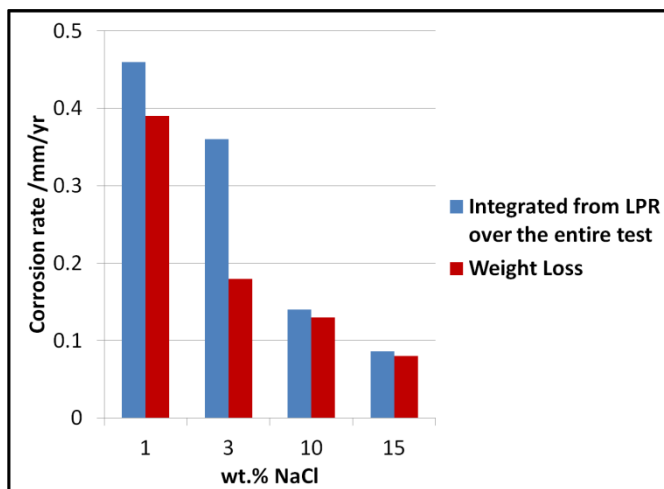


Figure 13: The general corrosion rate comparison for the four experiments defined in Table 1.

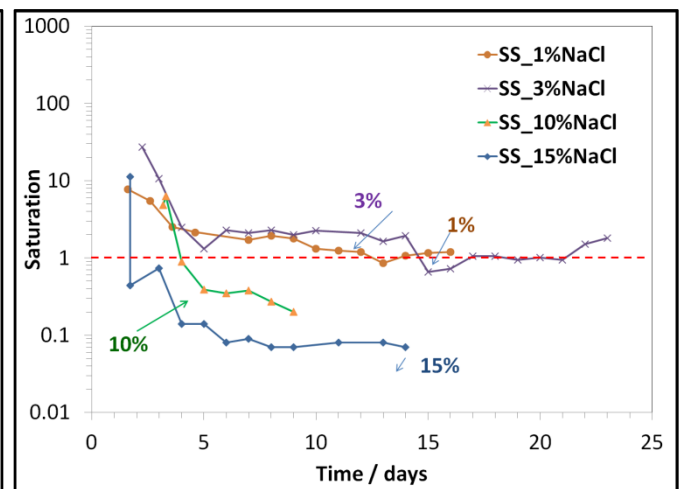


Figure 14: Comparison of the calculated FeCO_3 saturation values after adding chloride for the four experiments

Comparison of the calculated FeCO_3 saturation

Figure 14 shows the calculated FeCO_3 saturation values when adding chlorides in the four experiments. It was found that in the 1 wt. % and 3 wt. % NaCl solutions, the FeCO_3 saturation was never less than 1 and no FeCO_3 dissolution and localized corrosion occurred. However, in the 10 wt.% and 15 wt.% NaCl solutions, the FeCO_3 saturation decreased far below 1 and FeCO_3 dissolution occurred leading to localized corrosion.

As shown by Equation 2, the FeCO_3 saturation is directly related to the FeCO_3 solubility, i.e. $K_{sp}(\text{FeCO}_3)$, which is related to ionic strength. High concentration of NaCl increases the ionic strength which caused $K_{sp}(\text{FeCO}_3)$ to increase and then subsequently reduce the bulk FeCO_3 saturation.

Summary I

SEM cross-section and optical profilometry analysis results indicated that in the lower concentration NaCl aqueous solutions, no localized corrosion was detected; while in the higher concentration NaCl aqueous solutions,

localized corrosion was found. Therefore, it seems clear that an increase in NaCl initiated localized corrosion. However, it is not clear if this effect was due to increased chloride ion concentration, $[Cl^-]$, or the reason for localized corrosion was the change in ionic strength? To answer these questions, $NaClO_4$ solution was used instead of NaCl in subsequent experiments.

Part II: Experiments in a $NaClO_4$ solution

Why use perchlorate ($NaClO_4$)?

From Part I experiments, the results indicated that localized corrosion was found in higher concentrations of NaCl solutions where a large change in ionic strength (1 wt% \rightarrow 10 wt% or 15 wt%) occurred, but not in lower concentration of NaCl solution when a smaller change of ionic strength (0.1 wt% \rightarrow 1 wt% or 3 wt%) happened. This same change in ionic strength could be achieved with any type of salt. Therefore, it was hypothesized that using $NaClO_4$ to replace NaCl should also lead to the decrease in bulk $FeCO_3$ saturation and possibly initiate localized corrosion. $NaClO_4$ was chosen because it is inert and does not get involved in the (electro)chemical reactions.¹³

Corrosion behavior

Figure 15 shows the corrosion rate and corrosion potential changed with time. For the first two days, after additional Fe^{2+} was introduced, the corrosion rate decreased rapidly and became stable at around 0.1 mm/yr. This decrease in corrosion rate meant that a protective iron carbonate layer formed as confirmed by the increase in corrosion potential as seen in previous experiments. When more solid $NaClO_4$ crystals were added into the glass cell, the corrosion rate increased rapidly, but was then reduced again within 2 days. The corrosion potential had also decreased significantly, which indicated that the iron carbonate lost some of its protectiveness.

The variation of the saturation of $FeCO_3$ under conditions: 80°C (176°F), initial pH 6.6, pCO_2 0.53 bar, in a $NaClO_4$ solution, is shown in Figure 16. During the first two days when the $FeCO_3$ layer was forming, the saturation decreased from 745 to near 10, which shows that ferrous ions were consumed by precipitation of $FeCO_3$. After additional $NaClO_4$ was added into the system, the saturation of $FeCO_3$ decreased significantly to much less than 1 because of the solution ionic strength change.

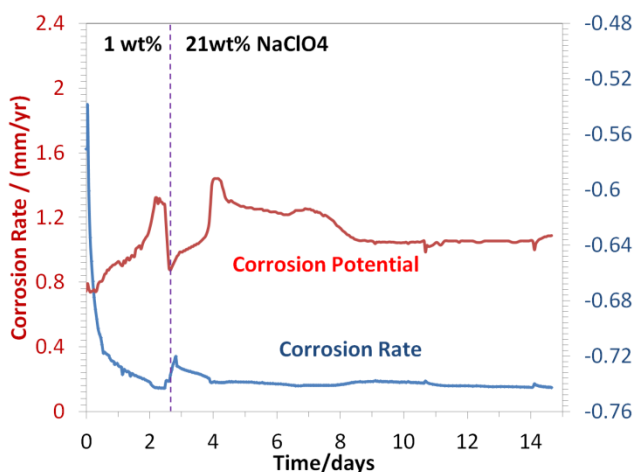


Figure 15: Variation of corrosion rate and potential with experiment time as determined by LPR measurements

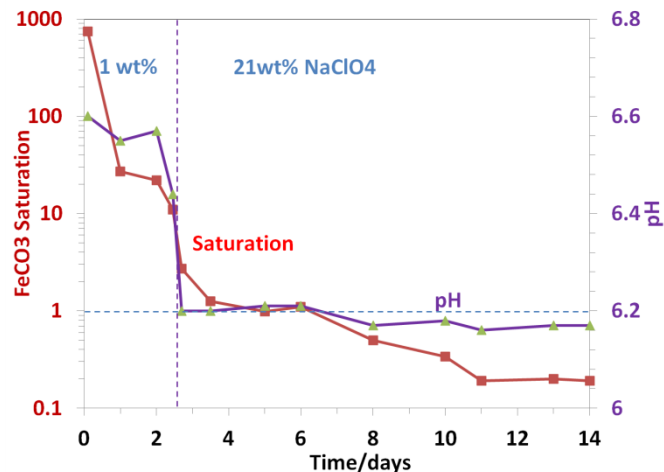


Figure 16: The variation of the saturation of $FeCO_3$ with time

SEM analysis

Figure 17 shows the surface morphology of the $FeCO_3$ layer after 2 days of $FeCO_3$ forming at following conditions: 1 wt.% $NaClO_4$ solution, 80°C (176°F), initial pH 6.6, pCO_2 0.53 bar. Figure 18 shows the cross-section of the same sample as seen in Figure 17. The $FeCO_3$ layer looks dense and uniform with a thickness of 6 μm . As compared to the layer formed in Experiment 3 of Part I (same conditions except with 1 wt. % NaCl, Figure 5 and Figure 6), the $FeCO_3$ layer appears topographically similar with a similar thickness.

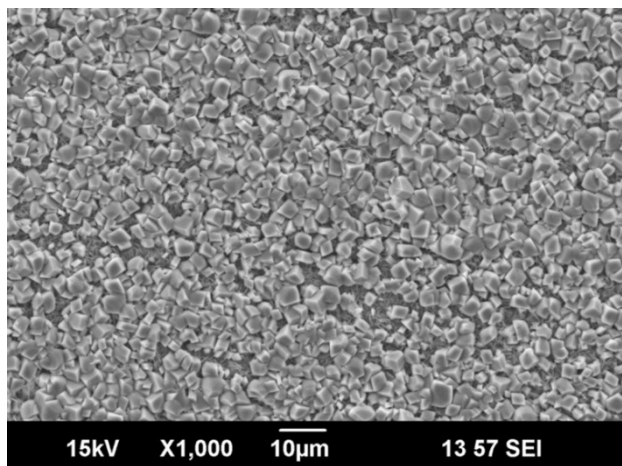


Figure 17: Surface morphology after FeCO₃ building process (1 wt. % NaClO₄ solution, 80 °C (176°F), initial pH 6.6, pCO₂ 0.53 bar)

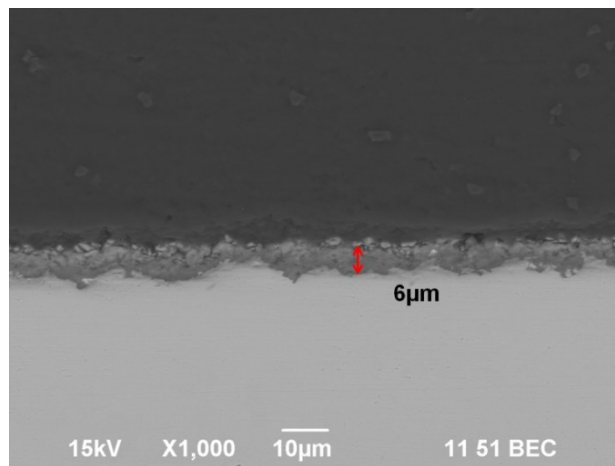


Figure 18: Cross-Section analysis after FeCO₃ building process (1 wt.% NaClO₄ solution, 80 °C (176°F), initial pH 6.6, pCO₂ 0.53 bar)

Figure 19 shows the surface morphology of the FeCO₃ layer after introducing additional NaClO₄ and monitoring for 6 days. Some areas were observed where FeCO₃ crystals structure was damaged which meant that FeCO₃ partially dissolved. Figure 20 shows the cross-section of the same sample as Figure 19. The variation of the NaClO₄ concentration also affected the protectiveness of the FeCO₃ layer since localized corrosion pits of up to 12 µm depth were found. Based on this penetration value, the pitting corrosion rate was equivalent to 0.73 mm/yr. The general corrosion rate obtained from LPR was 0.21 mm/yr. Thus, the pitting ratio was 3.5, which means that it was possibly a case of localized corrosion.

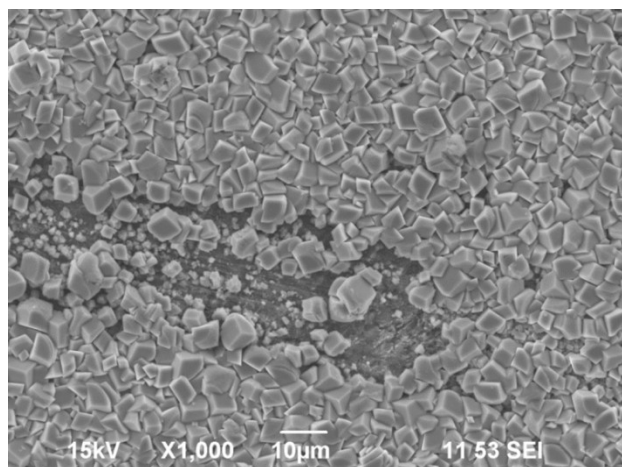


Figure 19: Surface morphology after FeCO₃ building process (1 wt. % NaClO₄ solution, 80 °C (176°F), initial pH 6.6, pCO₂ 0.53 bar)

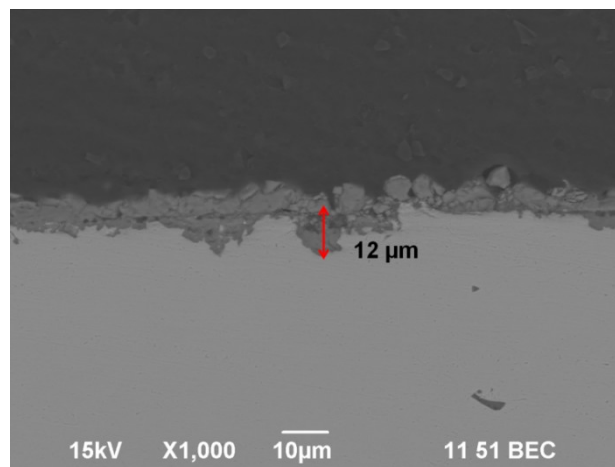


Figure 20: Cross-Section analysis after FeCO₃ building process (1 wt. % NaClO₄ solution, 80 °C (176°F), initial pH 6.6, pCO₂ 0.53 bar)

Figure 21 shows the surface morphology of the FeCO₃ layer after adding additional NaClO₄ for 12 days. Again, areas where observed where FeCO₃ crystals structure was damaged which indicates a partial dissolution of FeCO₃ layer. Figure 22 shows the cross-section of the same sample as shown in Figure 21; it also indicates a partial breakdown of the FeCO₃ layer with evidence of pitting to a depth of 19 µm. Based on this depth, the pitting penetration rate was 0.57 mm/yr. And the general corrosion rate calculated from weight loss was 0.17 mm/yr. Therefore, the pitting ratio was 3.4, which suggested that it could be localized corrosion.

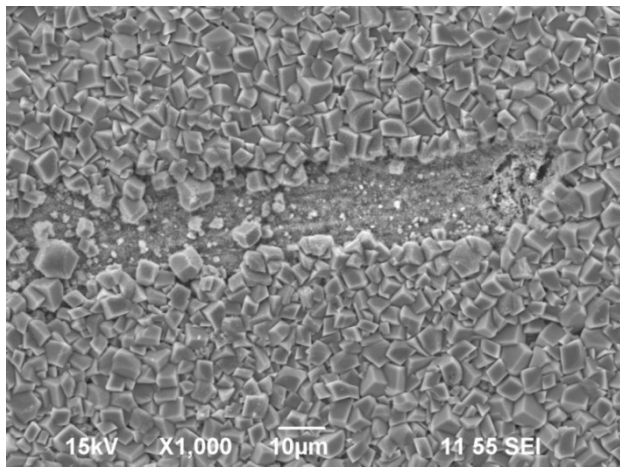


Figure 21: Surface morphology after FeCO₃ building process (1 wt. % NaClO₄ solution, 80 °C (176°F), initial pH 6.6, pCO₂ 0.53 bar)

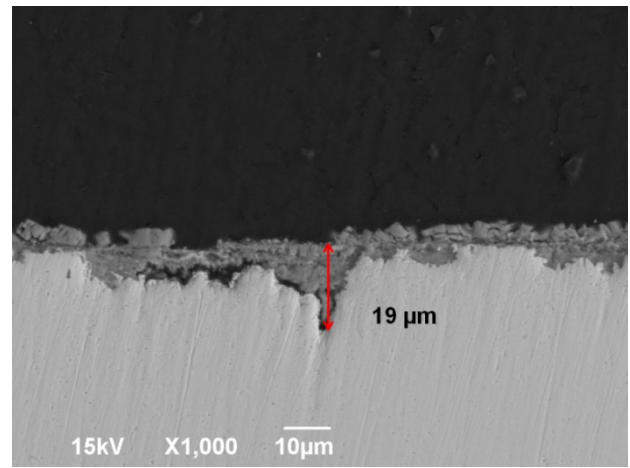


Figure 22: Cross-Section analysis after FeCO₃ building process (1 wt. % NaClO₄ solution, 80 °C (176°F), initial pH 6.6, pCO₂ 0.53 bar)

Optical profilometry analysis

Figure 23 shows the surface morphology after removal of the corrosion product layer using Clarke solution at the end of the experiment. The whole surface was scanned and the deepest pit observed was 15µm. Based on this depth, the pit penetration rate was 0.45 mm/yr. And the general corrosion rate calculated from weight loss was 0.17 mm/yr, so the pitting ratio was 2.7. Because the pitting penetration rate was larger than the general corrosion rate this might suggest localized corrosion. This result was consistent with the one obtained from SEM cross-section analysis.

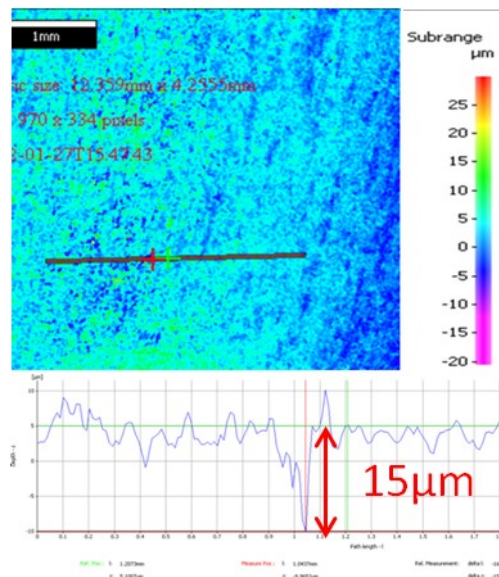


Figure 23: Optical Profilometry images and analysis of the steel surface after removal of corrosion product layer

XRD results

In order to check if the same corrosion products were formed in NaCl and NaClO₄ solution, XRD analysis was conducted. The XRD results shown in Figure 24 indicated that the corrosion product was composed of FeCO₃, Fe₂(CO₃)(OH)₂, with Fe being the substrate. These results agree with the results obtained in a NaCl solution, as shown in Figure 25.

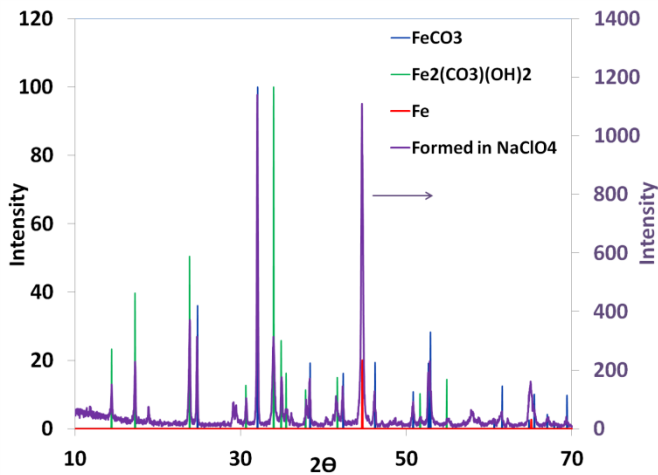


Figure 24: XRD results comparison for corrosion product formed in NaClO₄

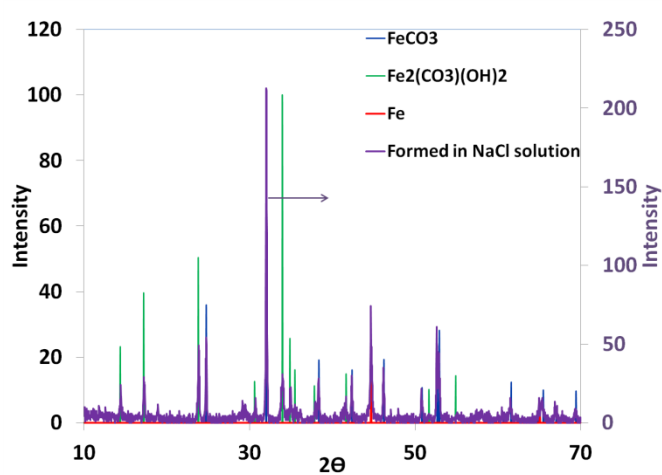


Figure 25: XRD results comparison for corrosion product formed in NaCl

Corrosion rate comparison

Figure 26 shows the comparison of corrosion rates for NaClO₄ and NaCl experiments. The general corrosion rates obtained from LPR were consistent with those calculated from weight loss. For both experiments, the pit penetration rates were much higher than the general corrosion rates. This suggested possible localized corrosion was initialized in both experiments.

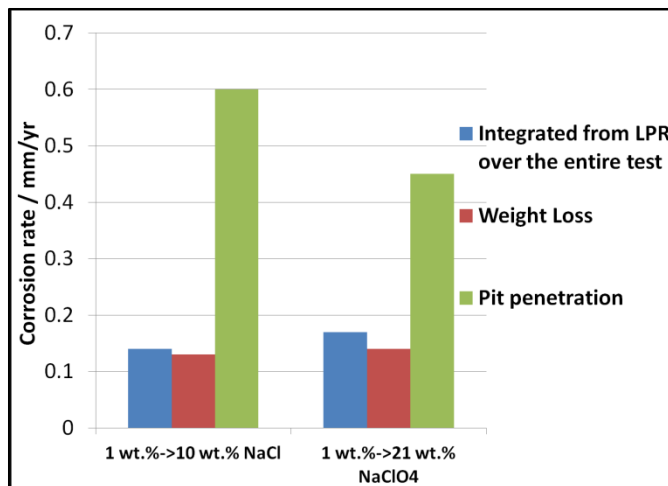


Figure 26: Corrosion rate comparison between NaCl and NaClO₄

Summary II

When NaClO₄ replaced NaCl, the saturation of FeCO₃ also decreased below 1 due to a solution ionic strength increase. Both the cross-section and profilometry analyses suggested that localized corrosion was initialized, which proved that partial breakdown of the iron carbonate layer on mild steel may occur due to changing in the solubility of iron carbonate caused by the changes in solution ionic strength.

CONCLUSION

This research focused on the effect of chlorides on the initiation of localized corrosion on carbon steel in CO₂ environments. It was found that in the lower concentration of NaCl solution with smaller change of ionic strength (Experiments 1 & 2), no localized corrosion was detected; but in the higher concentration of NaCl solution with larger change of ionic strength (Experiments 3 & 4), localized corrosion was found. Therefore, the effect of

solution ionic strength on the corrosion mechanisms related to initiation of localized corrosion was evident. A different salt, NaClO_4 was introduced to confirm the effect of ionic strength on initiation of localized corrosion. The results confirmed that initiation of localized corrosion could be caused by changing the solubility of iron carbonate through changes in the ionic strength of the solution, and was not directly caused by high chloride concentration.

ACKNOWLEDGEMENTS

The authors would acknowledge the Corrosion Center Advisory Board members for their financial support: BP, Champion Technologies, Chevron, Clariant Oil Services, ConocoPhillips, ENI S. P. A., ExxonMobil, Inpex Corporation, NALCO Energy Services, Occidental Petroleum Co., Petrobras, PETRONAS, PTT, Saudi Aramco, Total, TransCanada, MI-SWACO, HESS and WGIM. The authors also appreciate the help received for the use of the XRD equipment at the Center for Electrochemical Engineering Research, Department of Chemical and Biomolecular Engineering at Ohio University.

REFERENCES

- [1] S. M. Sharland, "A review of the theoretical modelling of crevice and pitting corrosion," *Corrosion Science* 27, 3 (1987), pp. 289–323.
- [2] J. Han, "Galvanic Mechanism of Localized Corrosion for Mild Steel in Carbon Dioxide Environments," Ohio University, 2009.
- [3] J. W. Palmer, J. W. Marsh, and R. C. Newman, "Evaluation of inhibitor performance for protection against localized corrosion," *Corrosion* 2002, paper no. 02288 (Houston, TX: NACE).
- [4] A. Turnbull, D. Coleman, A. J. Griffiths, P. E. Francis, and L. Orkney, "Effectiveness of Corrosion Inhibitors in Retarding the Rate of Propagation of Localized Corrosion," *Corrosion* 59, 3 (Mar. 2003), pp. 250–257.
- [5] H. Fang, "Low temperature and high salt concentration effects on general CO_2 corrosion for carbon steel," Master Thesis, Ohio University, 2006.
- [6] S. Netic, "Key issues related to modelling of internal corrosion of oil and gas pipelines—A review," *Corrosion Science* 49, 12(2007), pp. 4308–4338.
- [7] Y. F. Cheng, M. Wilmott, and J. L. Luo, "The role of chloride ions in pitting of carbon steel studied by the statistical analysis of electrochemical noise," *Applied Surface Science* 152, 3–4(Nov. 1999), pp. 161–168.
- [8] Y. Sun, K. George, and S. Netic, "The effect of Cl- and acetic acid on localized CO_2 corrosion in wet gas flow," *Corrosion* 2003, paper no. 03327 (Houston, TX: NACE).
- [9] G. S. Frankel, "Pitting Corrosion of Metals; A Review of the Critical Factors," *J. Electrochem. Soc* 145, 6(1998), pp. 2186–2198.
- [10] S. Netic and W. Sun, "Corrosion in Acid Gas Solutions," *Shreir's Corrosion*, (Oxford: Elsevier Science, 2010), pp. 1270–1298.
- [11] W. Sun, S. Netic, and R. C. Woollam, "The effect of temperature and ionic strength on iron carbonate (FeCO_3) solubility limit," *Corrosion Science* 51, 6(2009), pp. 1273–1276.
- [12] G01 Committee, "Guide for Examination and Evaluation of Pitting Corrosion," ASTM International, 1999.
- [13] B. W. Davis, M. J. Linman, K. S. Linley, C. D. Hare, and Q. Cheng, "Unobstructed electron transfer on porous polyelectrolyte nanostructures and its characterization by electrochemical surface plasmon resonance," *Electrochimica Acta* 55, 15(Jun. 2010), pp. 4468–4474.